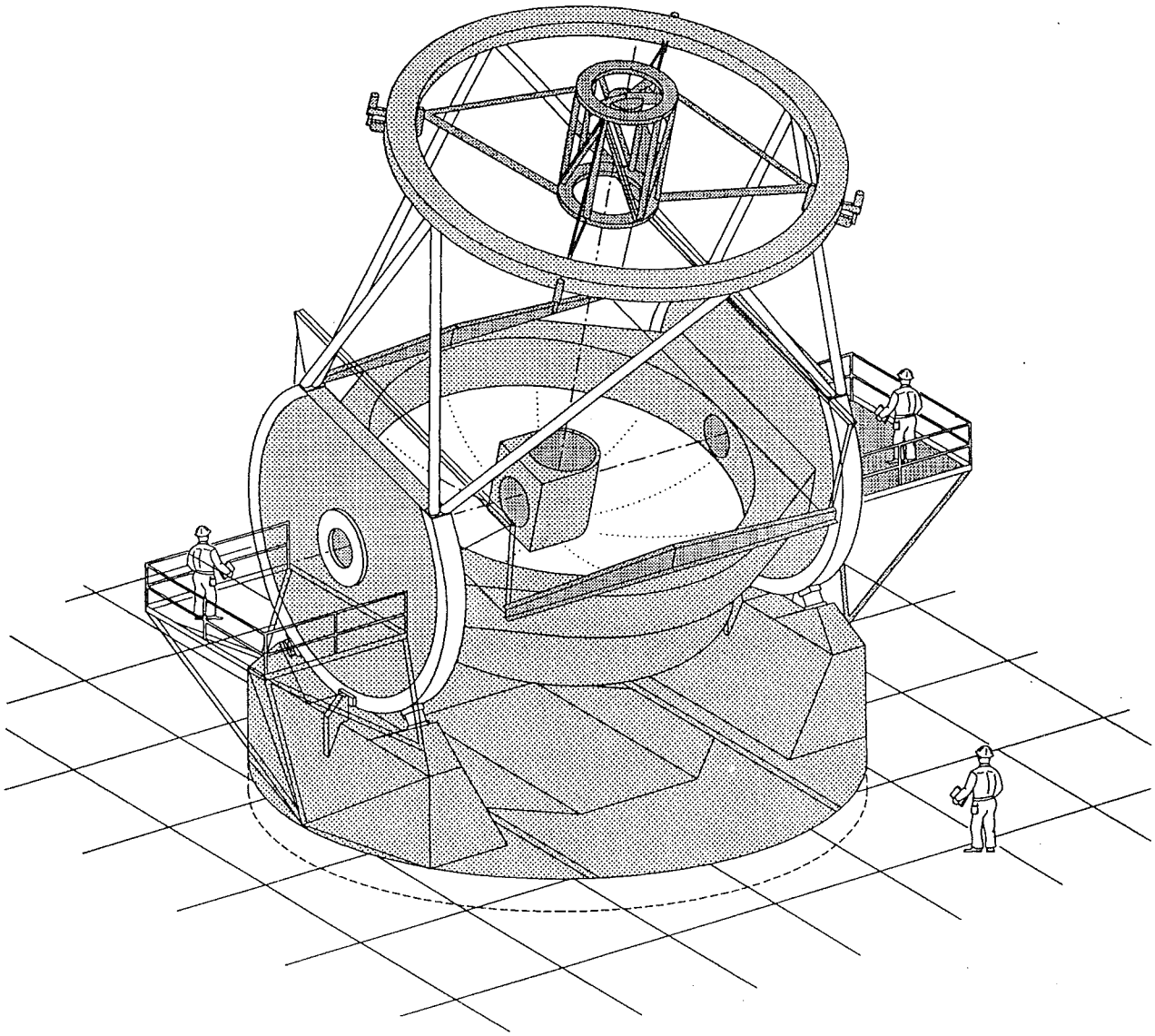

Magellan Project f11 Secondary Mirror
Preliminary Design of the Mirror, Supports, and Cell

Document No. 95SE0518

Steve Gunnels
Paragon Engineering
Tehachapi, California
and
Matt Johns
Carnegie Observatories
Pasadena, California

February 1995
No. 40

Magellan Project f11 Secondary Mirror
Preliminary Design of the Mirror, Supports, and Cell

Steve Gunnels
Paragon Engineering - Tehachapi, Ca. 93561

Matt Johns
Observatories of the Carnegie Institution of Washington - Pasadena, Ca. 91101

February 25, 1995

1. INTRODUCTION

The f11 Gregorian secondary for Magellan will be a lightweighted meniscus ~1.38 meters in diameter and ~17 cm thick. The lightweighting will be accomplished by machining as shown in Figure 1. The blank can be made from Zerodur or ULE. If made from Zerodur its weight will be approximately 187 kg; from ULE about 164 kg. Most of the 163 cells machined from the back side are hexagonal, 100 mm inside flats, with 33 mm inside corner radii. The ribs between cells are 5 mm thick. Exceptions to this are the undersize perimeter holes (holes 17, 18, and 19 in Figure 1), and the lateral support holes, indicated with "flag" no. 2. The axial support holes are hexagonal, but modified slightly from the typical holes. They are indicated with flag no. 3.

The axial support system consists of a vacuum augmented by three kinematic axial supports. The axial supports incorporate piezotranslators for fast steering. The three lateral supports are passive and kinematic. All supports are described in more detail in section 3. below.

2. MIRROR STRUCTURE

2.1 Horizon Gravity Figure

Due to the deep curvature of this concave optical surface, the lateral support system design was somewhat challenging. Three fundamentally different lateral support methods were evaluated with finite element analysis. Typical model graphics plots are shown in Figures 6 through 8. The first support method consisted of two radial supports at the perimeter of the mirror, with a third unspecified tangent support. The two main supports were placed 21° below the lateral centerline initially, then lowered to the 30° position. Both positions exhibited a tendency for the mirror to fold in half about the orthogonal centerline. The surface deviation from its unloaded condition was about 400 nm peak-to-peak. The RMS surface was 83 nm at best.

Next a central support hub was tried. Due to the close proximity of the c.g. plane to the front face at the center of the mirror, large local strain caused a "wave" shape to result at the surface. The spatial period of this wave was something greater than the diameter of the mirror. Its surface deviated from the unloaded shape by 480 nm pk-pk, or 68 nm RMS.

The next and much more successful lateral support analyzed consisted of two supports at the 61% radius points aligned to react horizon gravity, and a third orthogonal support at the center. The two horizon gravity supports then define Y translation and Z rotation for the mirror as defined in Figures 6 and 8. They are located on the c. g. plane. The orthogonal, or X translation support will likely be located slightly off the c.g. plane because of its close proximity to the face plate. This will cause very

slight forces to develop in the axial supports due to tracking acceleration.

The contour plot for this surface is shown as Figure 9. This support method results in two slight bumps at the surface near each support (actually, a 20 nm convex bump above a 20 nm concave trough when seen at horizon). The surface deviation is 40 nm pk-pk, or about 6 nm RMS. The Strehl ratio for this effect alone is 0.98 at 500 nm.

It should be noted that a number of variations and optimizations of this support method were analyzed. One was placing the two horizon gravity supports at two of the axial support cells. Another was moving them one cell inboard (toward the center of the mirror). A third involved placing the supports slightly off the c.g. plane and applying a compensating local moment with horizon gravity levers. All of these variations resulted in higher RMS surface errors and lower Strehl ratios.

2.2 Zenith Gravity Figure

Two load cases were run to predict mirror figure under zenith gravity loading. In the first the vacuum was applied to exactly balance the total weight of the mirror, with no force in the axial supports. The face and back plate thicknesses vary in each cell due to the tool shape as compared to the mirror curvature. Therefore, a conservatively thin average plate element thickness was used in the finite element model and additional mass added separately. This effect is most significant in the outer steep area of the mirror. This in combination with the 8 mm thick perimeter wall and thicker than average rib intersections cause the mirror to have greater density at the edge than at the center. In fact, these effects amount to a total of about 29 kg (16% of the mirror weight) of additional mass near the edge of the mirror. This was partially counteracted by additional vacuum load from the perimeter seal. Even so, the mirror figure exhibits about 200 nm of curvature which is predominantly a focus term.

It was determined that the low order aberrations could be removed by adjusting telescope focus without loss of image quality. The contour plot of the surface with Zernike terms 1 through 3 subtracted is shown as Figure 10. The print-through of the hexagonal cells is apparent. The amount of re-focus was small: about 4 microns.

In the second zenith gravity load case all of the mirror weight was taken on the axial supports (no vacuum). This resulted in 1500 nm of trefoil which is scalable against the vacuum error. To limit surface deflections to 40 nm it was determined that the vacuum must be controlled within 2%, or to a tolerance of about 2 mm of water.

2.3 Stresses in Glass

Considerable design and analysis was performed to assure that stresses in the glass would be low. The goal for the maximum working stress in the glass was set as 200 psi, assuring a large structural safety factor for either ULE or Zerodur.

A model such as shown in Figure 6 was used to determine global stresses (remote from the supports) under zenith gravity with the vacuum turned off. The maximum stress here was 96 psi. The local stress near the support under this same load case was 156 psi. This was determined with model SM16, shown in Figure 7. The stress occurs in the fillet radius between the back plate and ribs.

Since the lateral supports will bond to the glass the potential exists for stresses to develop due to thermal loading. That is, if the device that is bonded to the glass, in combination with the adhesive

itself have a net finite coefficient of thermal expansion, some stress will develop due to the 56 °C design ambient survival temperature range. Considerable work was done to eliminate or minimize this effect, which is summarized in section 3 below. Finally, an athermal design was created which nominally should cancel this effect. However, due to material CTE variations and design and manufacturing tolerances, some residual thermal effect will exist. From model SM16 it was conservatively determined that the maximum stress in the glass under horizon gravity with no thermal effect would be 142 psi. Using the preliminary design for the lateral supports described below, an additional 30 psi will develop per 10% thermal error due to tolerances, for the full 56 °C temperature swing. That is, if actual CTE's vary in such a way as to cause a 10% difference in the expansion of the adhesive and contraction of the support, the actual stress should be 142 + 30 = 172 psi. If necessary, some testing can be performed in the detail design phase to limit these errors to assure that the stress in the glass doesn't exceed 200 psi.

The stress at the X lateral support was calculated to be 214 psi under a .4 g earthquake, and would be slightly higher due to the same thermal effect resulting from CTE variations. If necessary, this stress can be reduced further by altering of the attachment pad geometry for this support only.

From the above we have concluded that we can limit the stress in the glass to 200 psi under all normal operating load conditions. Stresses under combined operating and seismic conditions may slightly exceed 200 psi but even these can be reduced further if necessary during the detail design of the supports.

3. SUPPORTS

3.1 Lateral Supports

The lateral supports are shown in Figures 3 and 4. Each support consists of a blade flexure which attaches at its back end to the cell and an athermal support which connects the other end of the blade to the glass. The athermal support includes (8) small milled flexures as shown so that it only has X and Y translation stiffness. The X translation stiffness for the Y lateral supports is canceled by the milled flexure at the other end of the blade, and conversely with the X lateral support.

Considerable design was done on the support to limit stresses in the glass due to thermal effects. The geometry is such that the difference in the positive CTE's of the aluminum and invar causes the assembly to act as though it had a negative CTE. Therefore, the final design is athermal in the sense that, for any temperature rise, thermal expansion of the adhesive (assumed to be 27.5E-5/°C) is just canceled by an opposite contraction of the invar/aluminum fitting. As shown, each 25 mm square pad uses 2 mm thick Dow Corning 93-076 RTV silicone adhesive. The relatively thick silicone was used to provide some compliance and thus limit glass stresses due to CTE tolerances. Conversely, with this thickness and geometry each silicone pad, with a shape factor of 3.13, was estimated to have a stiffness of 45,000 lb/in. With two pads in parallel, the net 90,000 lb/in. pad stiffness combines with an estimated 50,000 lb/in. stiffness for each blade to define a net stiffness of 32,000 lb/in. for each lateral support. Therefore, the silicone adhesive pads are soft enough to limit thermal stresses, yet stiff enough to provide adequate modal performance (summarized below).

3.2 Axial Supports

The axial support design is shown in Figure 5. It includes an invar attachment fitting which clamps top and bottom against the glass flange machined into the back plate of each axial support hole. The fittings that interface directly to the glass will either be teflon-lined invar or they will bond to the

glass using silicone adhesive. The invar fitting includes a spring-loaded bronze plunger. This plus the spring-loaded split ring act to protect the mirror from inadvertent instantaneous forces from the piezotranslator.

Above the invar attachment fitting is the low voltage piezotranslator. Although this model is capable of significant tension loads, it is being preloaded to assure that it is always in compression. Just beyond each end of this assembly is a flexured tip, which assures that the piezotranslator sees virtually zero moment. Finally, the upper flexured tip connects to the load cell via a rod, adapter, and cap which are provided for ease of assembly.

The net stiffness of each axial support assembly was estimated to be about 150,000 lb/in., determined approximately equally by the piezotranslator and the fittings which connect it at its top and bottom ends. This was found to provide very high axial resonant frequencies, discussed below.

4. CELL

4.1 Cell Structure

The cell is shown in Figure 2. It provides a platform for the 6 degree-of-freedom support system for the mirror, reacts the vacuum load, and connects the assembly to the telescope cage structure. It was originally planned to be made mainly from 1/4" steel plate. However, this in combination with the final mirror design proved to be quite heavy. The f11 assembly will be removed from the telescope frequently. Since the optics support structure (OSS) will be rebalanced by the powered counterweight system, this additional weight adds to the variable moment required of the counterweights. Therefore, it became apparent that a lighter cell would be very desirable.

The main structural requirement for the cell is to define high primary mode resonant frequencies, especially considering that the axial actuators will be fast-steering with a 20 Hz sinusoid. Therefore, a much lighter aluminum cell was compared to the steel design using modal performance as the criterion. The frequencies (in Hz) were:

MODE	1/4" STEEL CELL	1/4" ALUMINUM CELL
X translation	28.5	26.5
Z rotation	29.0	27.3
Y translation	34.9	31.1
Z translation	93.2	78.7
X tilt	99.4	90.7
Y tilt	99.5	91.5

From the above it is apparent that little penalty is paid in modal performance for the aluminum cell. Since the 1/4" aluminum cell is 210 kg lighter than a 1/4" steel cell, it will be used with the f11. The total weight for the assembly, including the mirror, cell, and support system, is estimated to be 348 kg (767 lbs).

It is anticipated that the lateral supports can be stiffened somewhat during the detail design phase. A reasonable goal for the first primary mode resonance for the f11 assembly (mounted to a rigid support) would be 30 to 35 Hz.

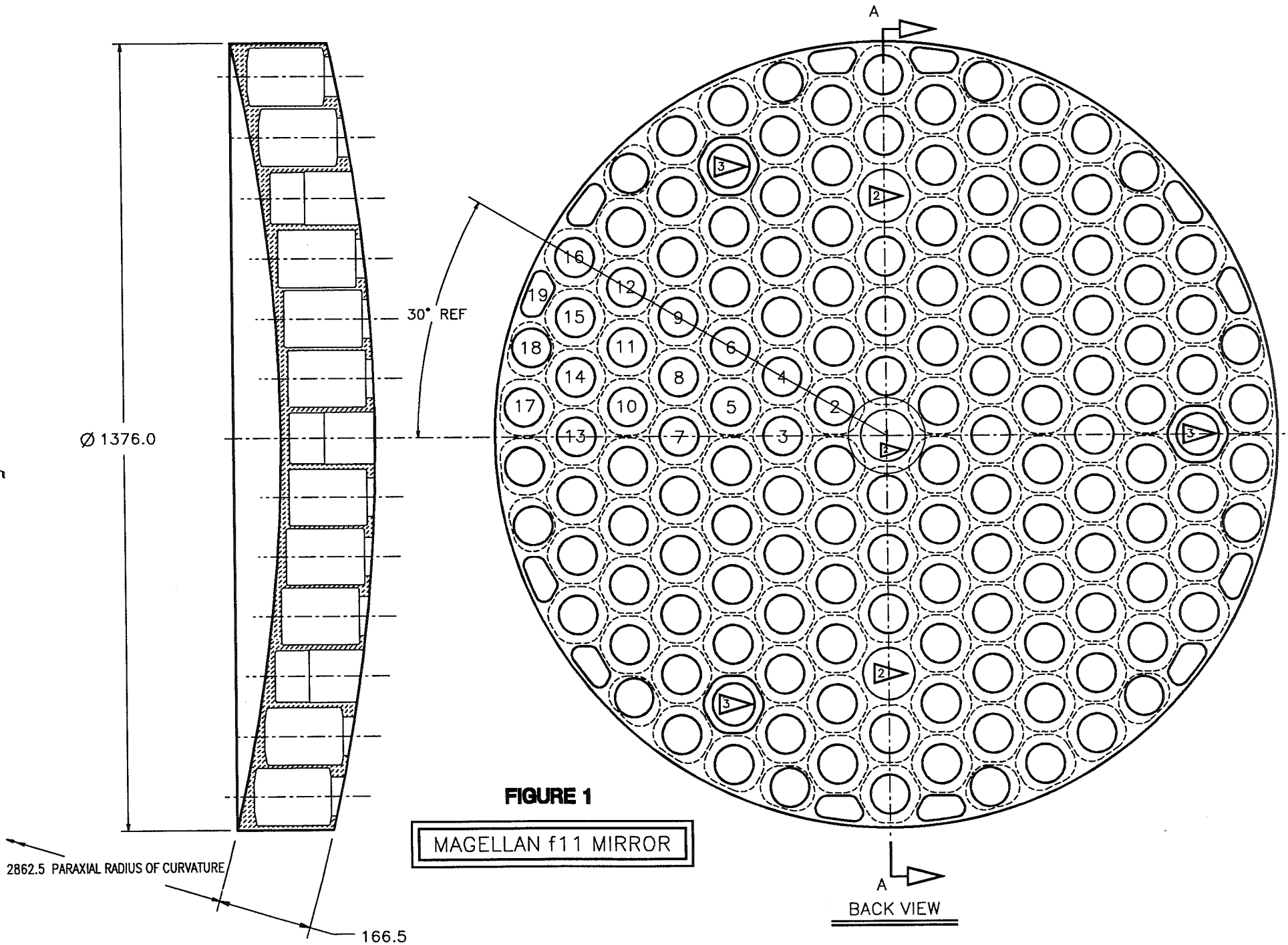

FIGURE 1

MAGELLAN f11 MIRROR

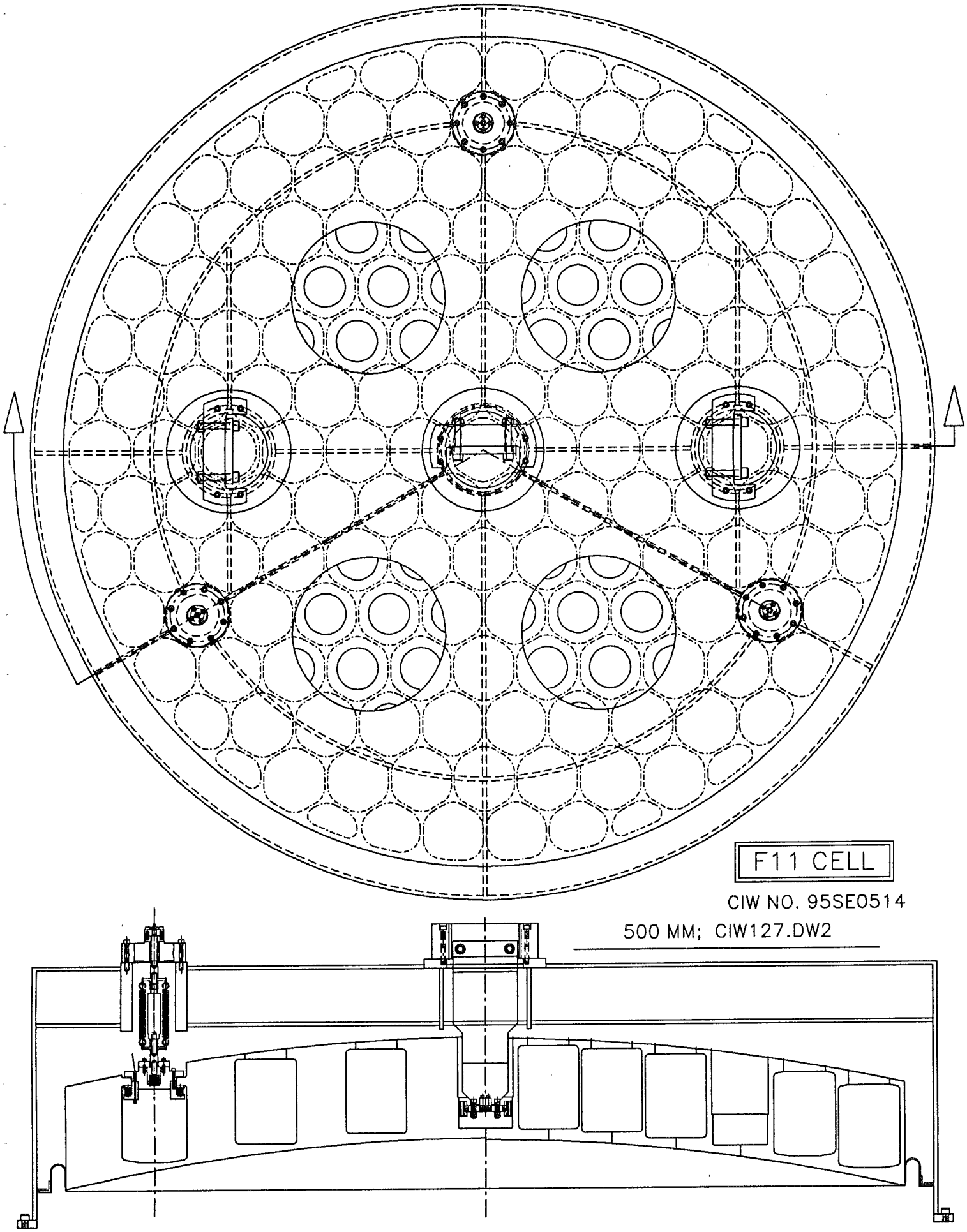

FIGURE 2

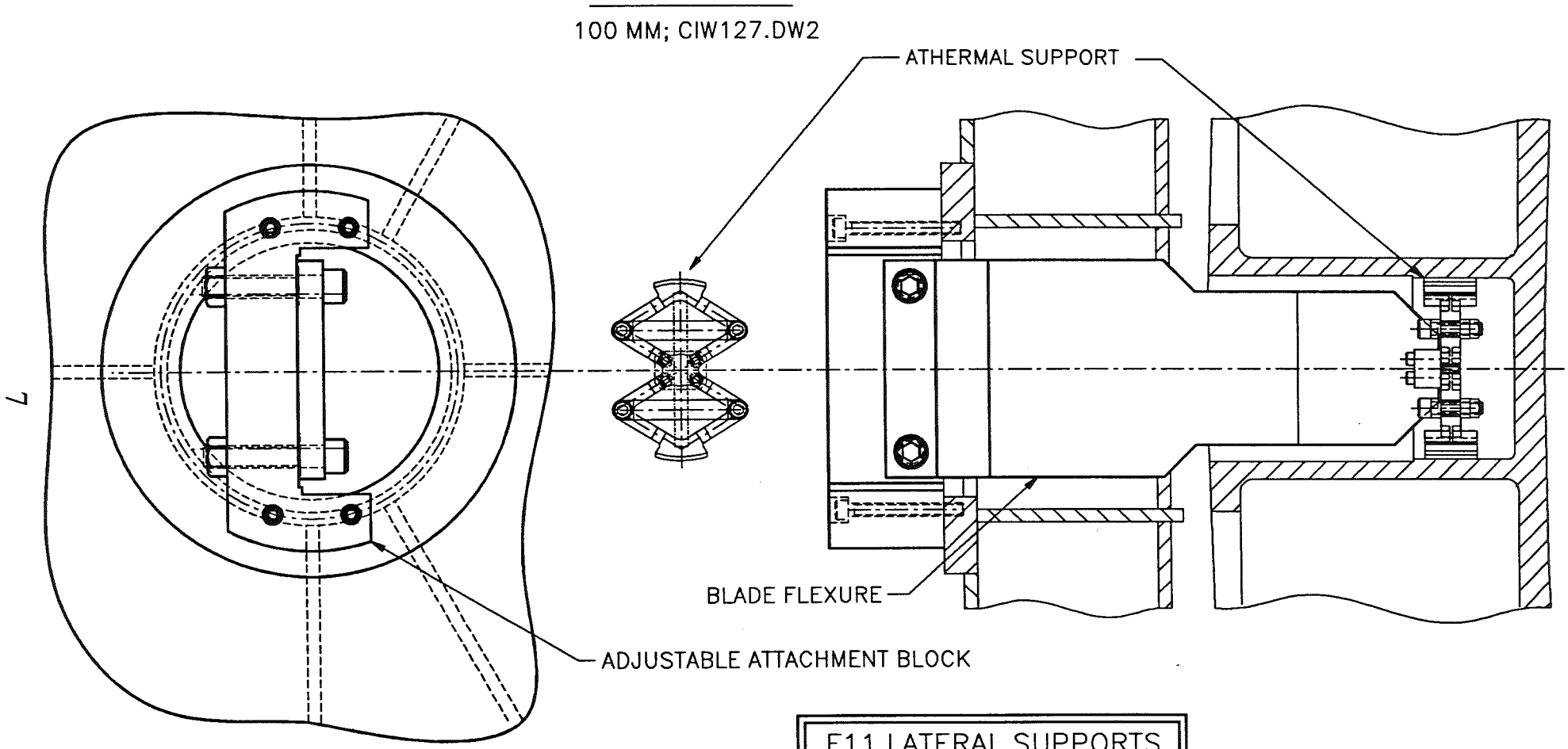
100 MM; CIW127.DW2
ATHERMAL SUPPORT
BLADE FLEXURE
ADJUSTABLE ATTACHMENT BLOCK
F11 LATERAL SUPPORTS
CIW NO. 95SE0515 SMG 2-17-95

FIGURE 3

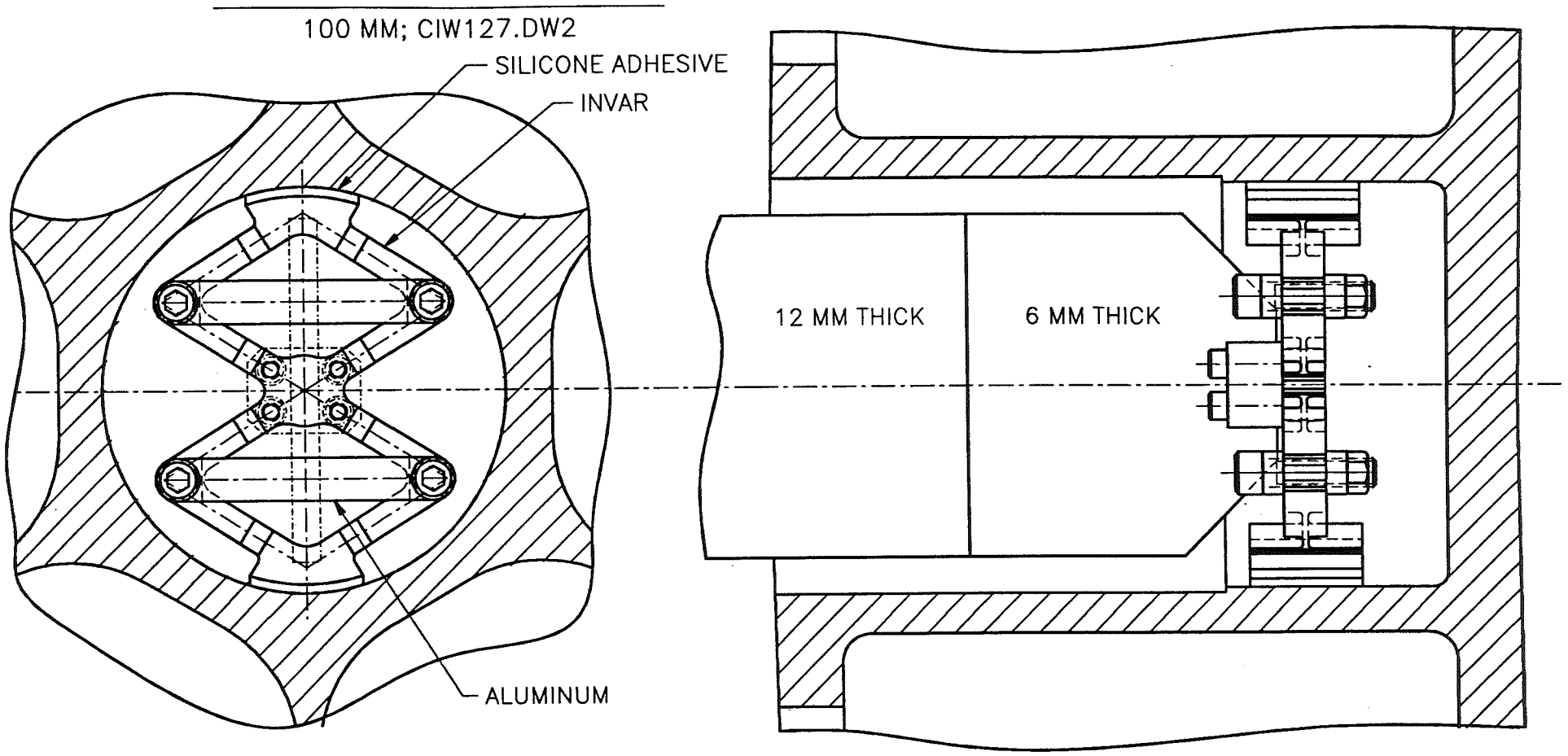

F11 LATERAL SUPPORTS

REF CIW NO. 95SE0514 SMG 2-17-95

FIGURE 4

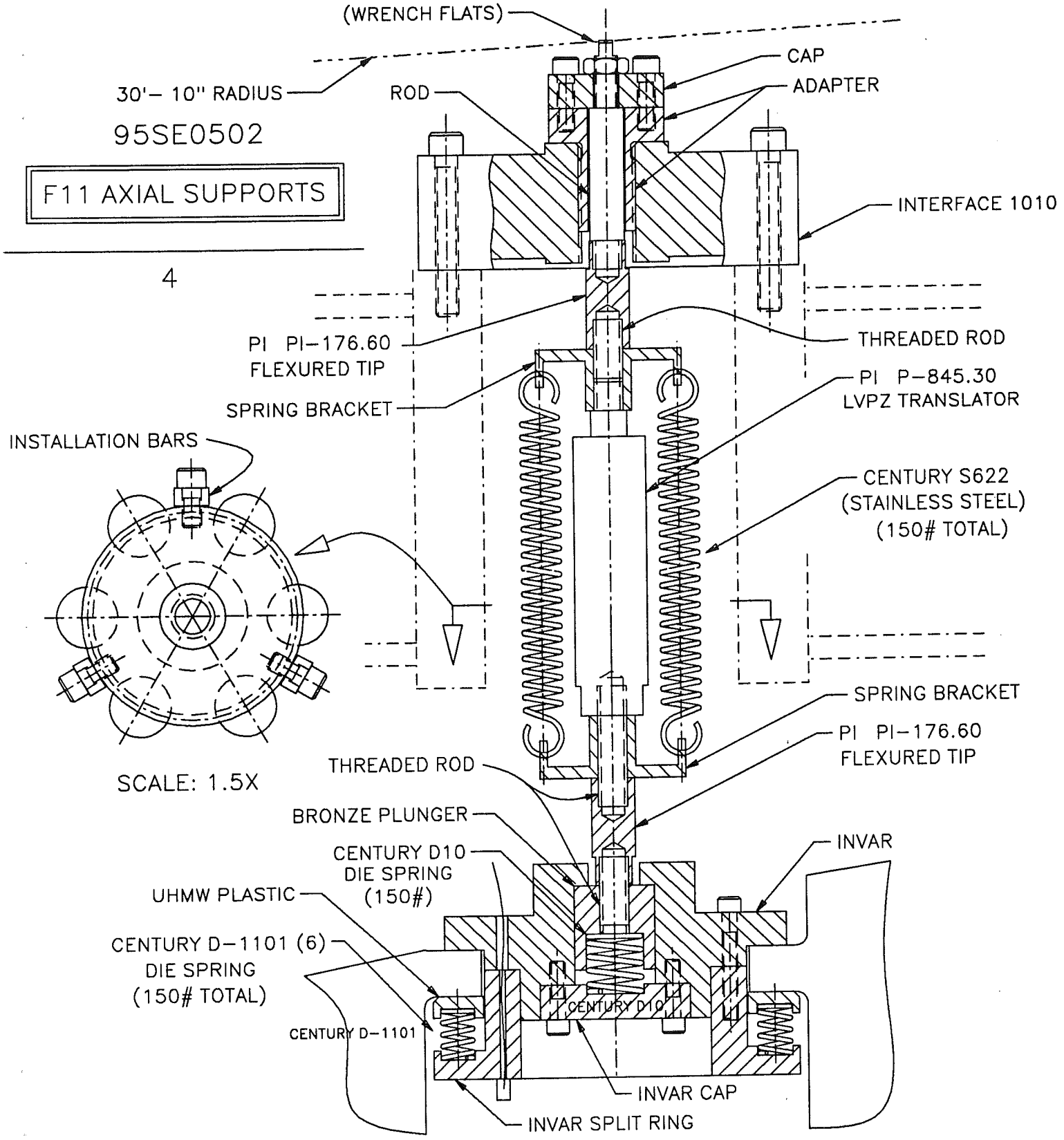
(WRENCH FLATS)
30'– 10" RADIUS
95SE0502
F11 AXIAL SUPPORTS
4
ROD
CAP
ADAPTER
INTERFACE 1010
PI PI–176.60
FLEXURED TIP
THREADED ROD
SPRING BRACKET
PI P–845.30
LVPZ TRANSLATOR
INSTALLATION BARS
CENTURY S622
(STAINLESS STEEL)
(150# TOTAL)
SCALE: 1.5X
SPRING BRACKET
PI PI–176.60
FLEXURED TIP
THREADED ROD
BRONZE PLUNGER
INVAR
CENTURY D10
DIE SPRING
(150#)
UHMW PLASTIC
CENTURY D–1101 (6)
DIE SPRING
(150# TOTAL)
CENTURY D10
CENTURY D–1101
INVAR CAP
INVAR SPLIT RING

FIGURE 5

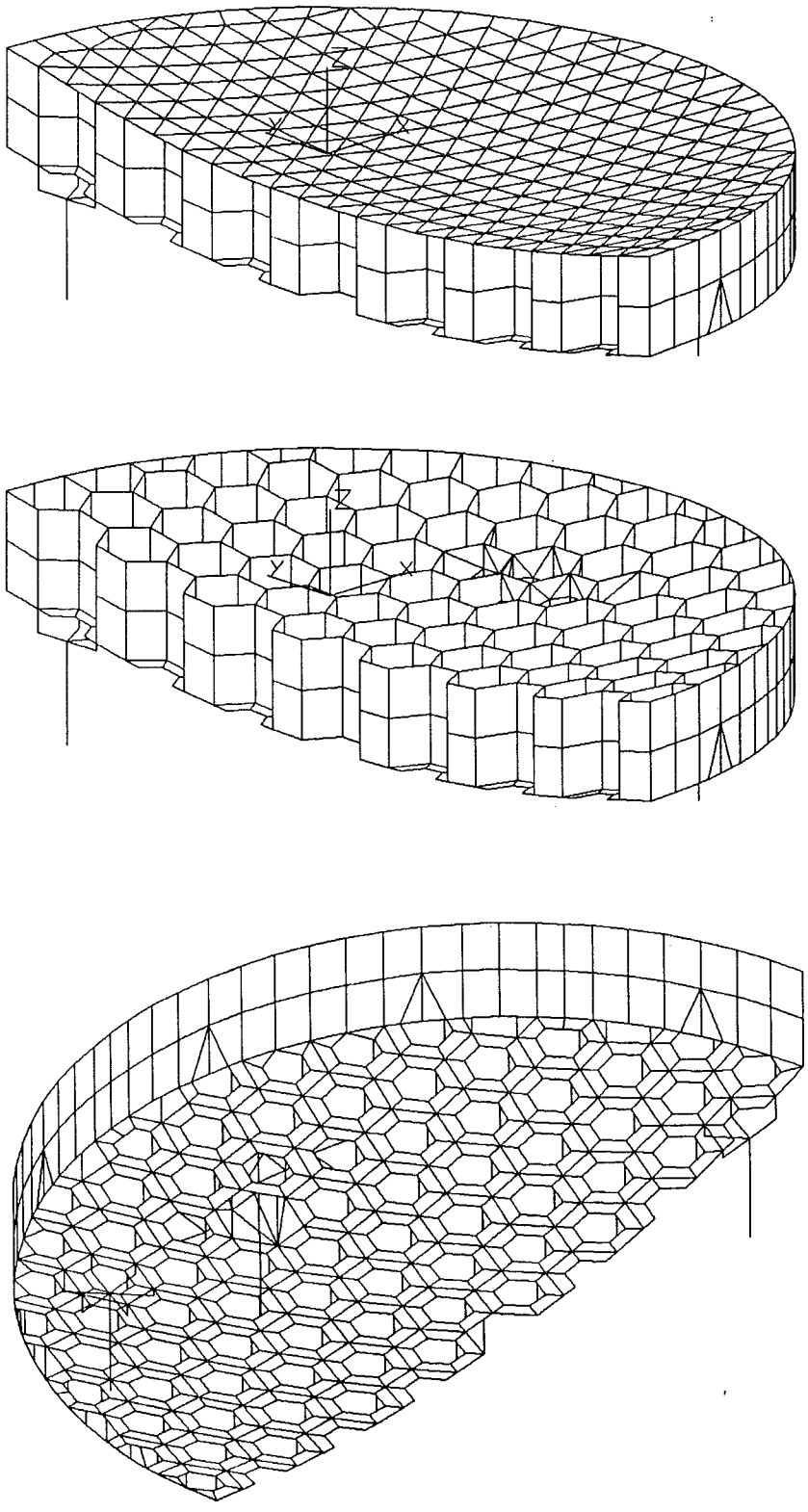

FIGURE 6

Model SM30, the static analysis used to determine mirror figure under zenith gravity with perfectly balanced vacuum (no load on axial supports). SM30 was also used to determine figure errors (trefoil) as a function of vacuum error. Front quartering views with and without front face elements are shown in the top two views. The back quartering view below indicates the hole pattern provided for tool access during machining.

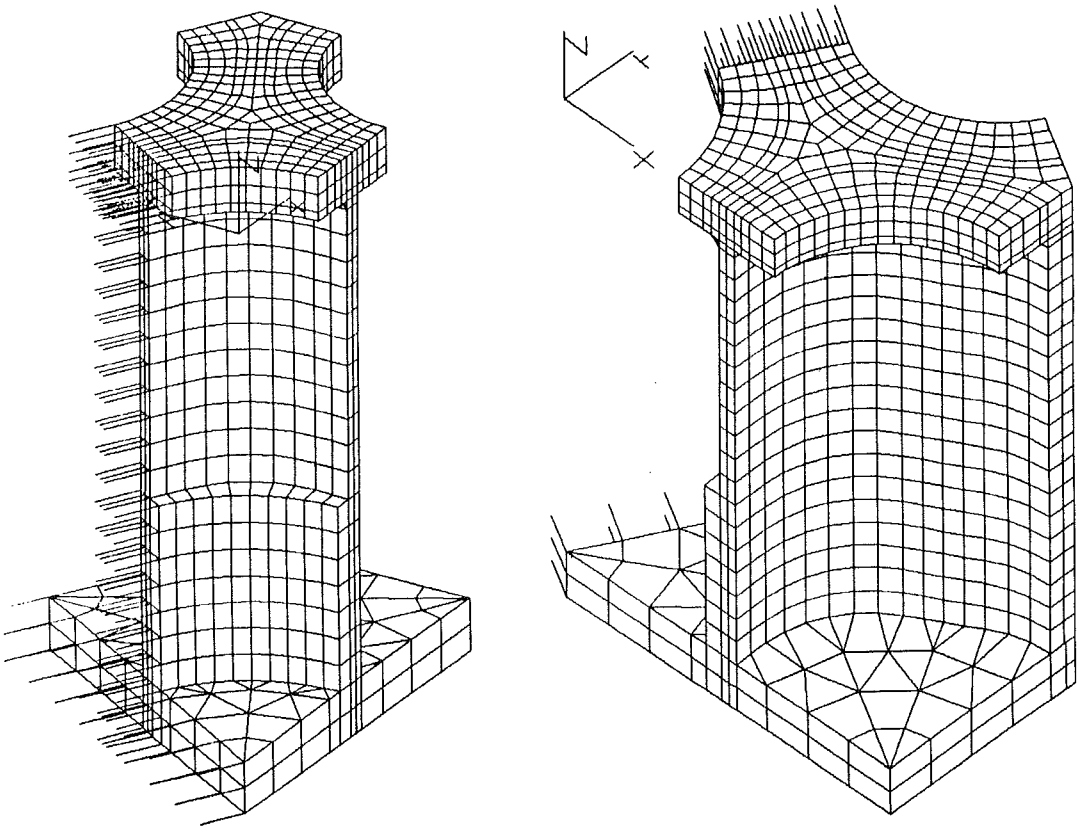

FIGURE 7

Model SM16, used to determine local stresses from the axial and lateral supports and stiffness of the mirror at the axial supports.

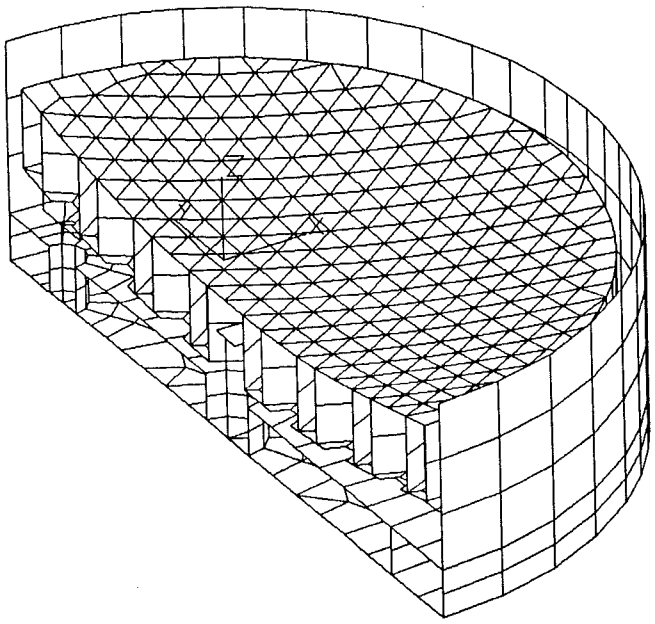

FIGURE 8

One-half of model SM31A, the modal analysis of the complete assembly that attaches to the telescope cage structure.

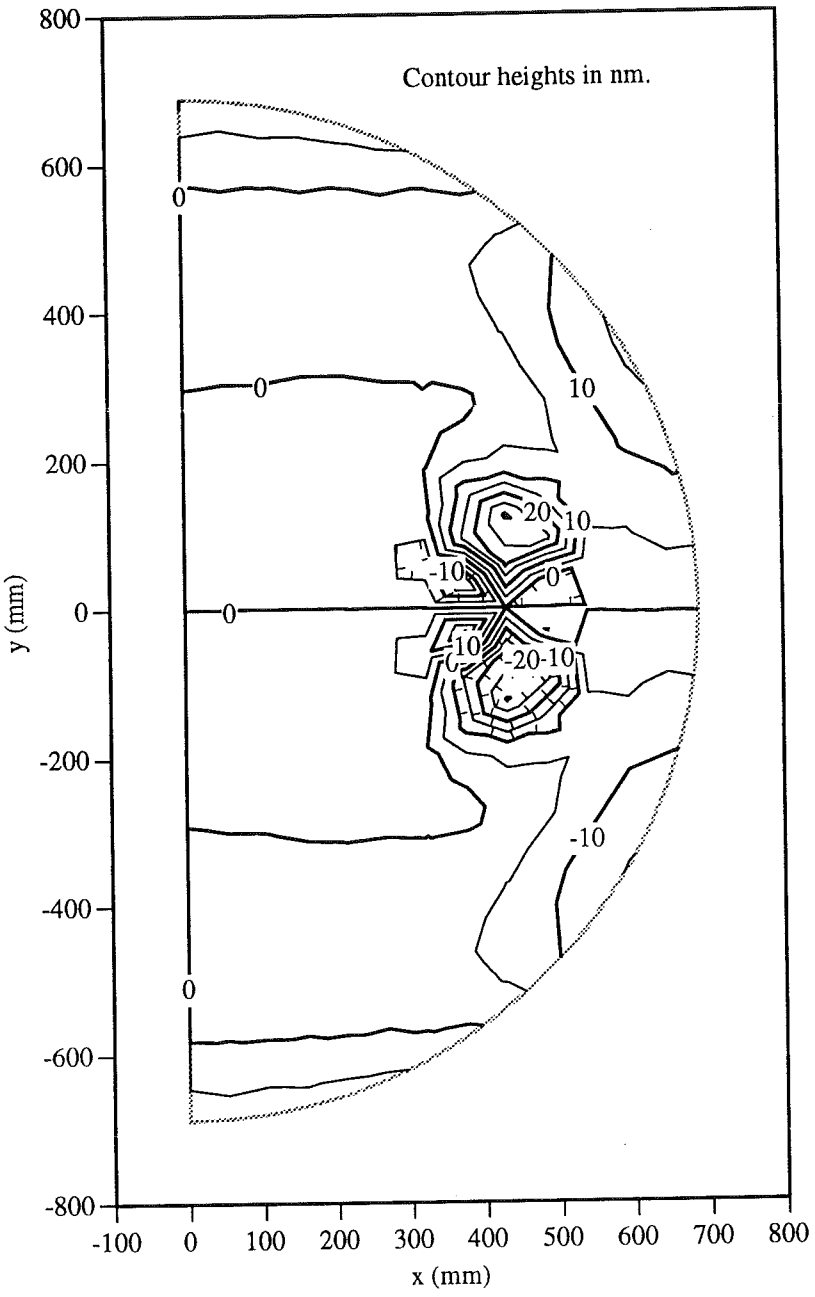

Figure 9. Surface deflection due to the lateral supports with the telescope pointed at the horizon. Model SM29.

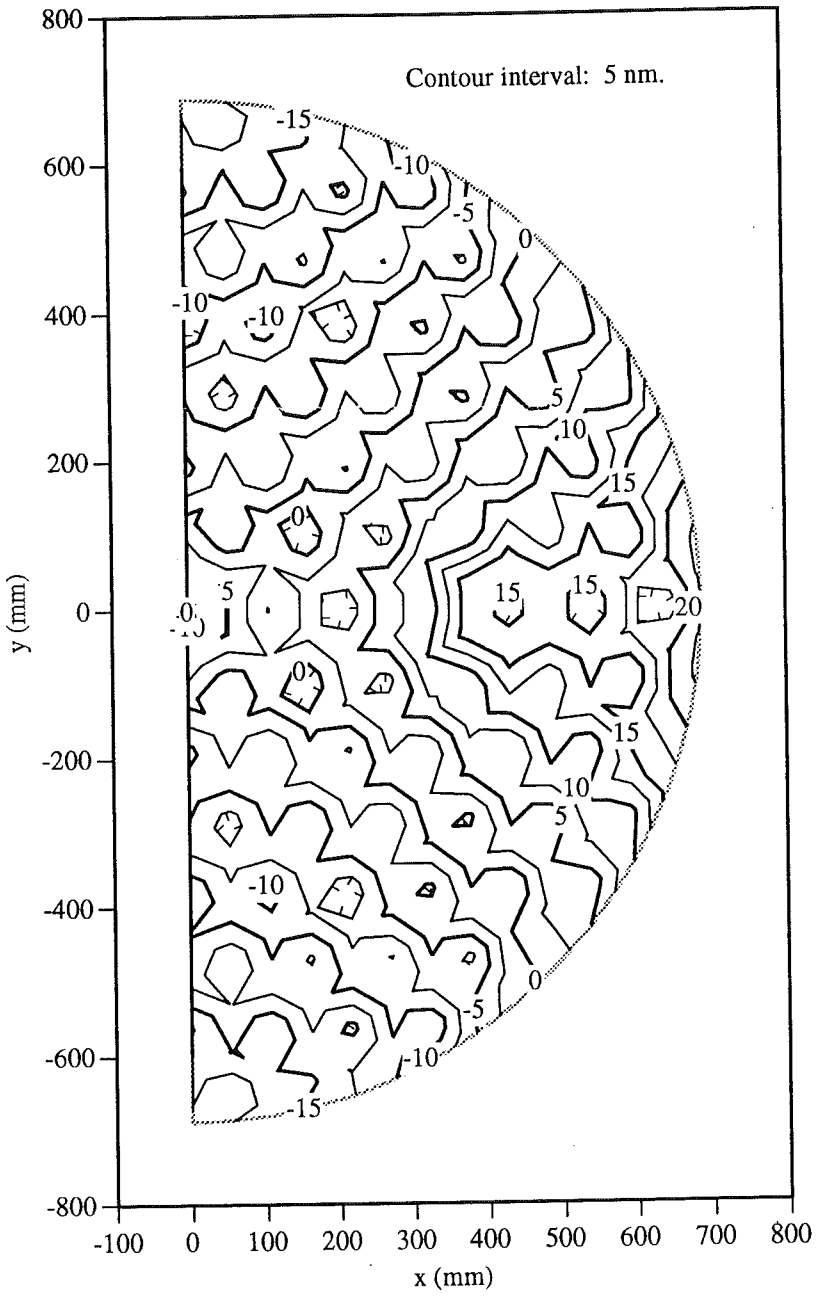

Figure 10. Surface deflection due to the axial supports with the telescope pointed at the zenith. Tilt, focus and piston are removed. Model SM30.